ChemComm

COMMUNICATION

View Article Online
View Journal

Check for updates

Cite this: DOI: 10.1039/d4cc06370h

Received 3rd December 2024,
Accepted 12th February 2025

DOI: 10.1039/d4cc06370h

rsc.li/chemcomm

Cellular uptake mechanisms of a diselenide-based ROS-responsive nanocarrier in oxidatively stressed colon cells†

Wanqi Liang,[a] Dong Li,[d] Jinheng Hao,[a] Wenli Dai,[a] Bo-Bo Zhang *[abc] and Qiongqiong Yang *[abc]

Here, we demonstrate that a diselenide-based ROS-responsive nanocarrier exhibits a highly sensitive response to ROS and excellent ROS scavenging activity. Mechanism studies indicate that it can be efficiently taken up by oxidatively stressed colon cells through folate receptor-mediated endocytosis, underscoring its potential for targeted drug delivery in treating colon diseases.

Reactive oxygen species (ROS) refer to a group of highly reactive ions and free radicals, including but not limited to superoxide (O^{2-}), hydroxyl radicals ($^{\bullet}OH$), hypochlorite ions (OCl^-), hydrogen peroxide (H_2O_2), and singlet oxygen ($^1O_2$).[1] Generally, normal cells generate low levels of ROS that are important for regulating cell signaling pathways and promoting cell proliferation. In contrast, oxidatively stressed cells produce increased levels of ROS, which can cause non-specific damage to proteins, lipids, and DNA, ultimately leading to several diseases including colon diseases, autoimmune disease, cardiovascular disease, and so on.[1]

These abnormal biochemical changes at disease sites have inspired researchers to leverage unbalanced ROS levels for developing target-specific drug delivery systems.[2] By utilizing ROS-responsive moieties and linkers, various ROS-responsive drug delivery systems have been developed that can activate and release drugs on demand at the disease site. Among these, polymer nanoparticles, formed through spontaneous self-assembly of amphiphilic block copolymers, are widely recognized as efficient carriers for the delivery of a wide range of therapeutic agents.[3] The incorporation of ROS-responsive units into polymeric nanoplatforms for controlled drug release offers promising nanotherapeutic carriers for targeting diseases associated with oxidative stress. Additionally, the low bond energy (172 kJ mol^{-1}) of diselenide (Se–Se) makes diselenide-containing polymers particularly sensitive under mild stimuli conditions, encouraging researchers to explore the diselenide bond for developing stimuli-responsive drug delivery systems.[4,5]

Although a host of diselenide-containing polymer nanocarriers have been developed over the past decade, it remains unclear which mechanisms precisely orchestrate diselenide-containing polymer nanocarrier-mediated cargo delivery to recipient cells. Previous studies suggested that the cell entry of nanoparticles is mainly through macropinocytosis, clathrin-dependent endocytosis, caveolin-dependent endocytosis, and clathrin- and caveolin-independent endocytosis.[6] However, our previous study found that a diselenide-containing polymer nanocarrier was not taken up by oxidatively stressed HT-29 cells *via* these reported endocytosis mechanisms. We hypothesized that the membranes of oxidatively stressed colon cells may highly express several transport proteins that can efficiently mediate the endocytosis of diselenide-containing polymer nanocarriers.

In this proof-of-concept study, we investigate in detail the role of oxidative stress in the cellular uptake of diselenide-containing polymer nanocarriers using diselenide-containing carboxymethyl cellulose (CMC-Se) as a model. The synthetic routes of CMC-Se are shown in Scheme S1 (ESI†). The chemical structures of intermediates were characterized by ^{1}H NMR (Fig. S1, ESI†). As shown in Fig. S1a (ESI†), Se–NHBoc showed characteristic proton resonance signals at 7.56–7.16 ppm (a, *Fmoc*, $C_{12}H_8$), 4.49–4.12 ppm (a, *Fmoc*, –CH–CH$_2$–), 3.71–3.51 ppm (c, –CH$_2$–NHBoc, –Se–CH$_2$–CH$_2$–NH–), 3.23–2.80 ppm (c, –Se–CH$_2$–CH$_2$–NH–), 1.98–1.67 ppm (d, –CH$_2$–CH$_2$–CH$_2$–), and 1.58–1.33 ppm (b, Boc), confirming that 2,2′-diselanediyldiethanamine was successfully connected to *Fmoc*-D-Lys(Boc)–OH. The Se–NH$_2$ ^{1}H NMR spectrum (Fig. S1b, ESI†) showed characteristic proton resonance signals at 8.18–7.23 ppm (a, *Fmoc*, $C_{12}H_8$), 4.51–4.19 ppm (a, *Fmoc*, –CH–CH$_2$–), 3.76–3.52 ppm (c, –CH$_2$–NH$_2$, Se–CH$_2$–CH$_2$–NH–), 3.30–2.77 ppm (c, Se–CH$_2$–CH$_2$–NH–), and 1.97–1.60 ppm (d, –CH$_2$–CH$_2$–CH$_2$–), confirming that the Boc protecting group was removed from Se–NHBoc. As shown in Fig. S2 (ESI†), the characteristic peaks of CMC and Se–NH$_2$ appeared in the ^{1}H NMR spectrum of CMC-Se, confirming the successful

---

[a] Department of Biology, College of Science, Shantou University, Shantou 515063, Guangdong, China. E-mail: qiongqiongyang@stu.edu.cn
[b] Guangdong Provincial Key Laboratory of Marine Biotechnology, Institute of Marine Sciences, Shantou University, Shantou, 515063, China
[c] Shantou Key Laboratory of Marine Microbial Resources and Interactions with Environment, Shantou University, Shantou, 515063, China
[d] Chemistry and Chemical Engineering Guangdong Laboratory, Shantou 515031, China

† Electronic supplementary information (ESI) available. See DOI: https://doi.org/10.1039/d4cc06370h

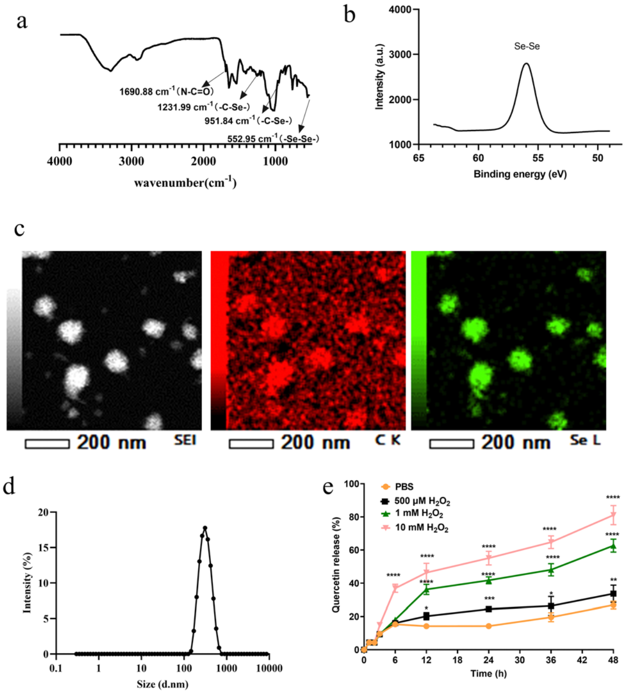

Fig. 1 FTIR analysis of CMC-Se (a). XPS analysis of CMC-Se (b). EDX analysis of CMC-Se (c). DLS analysis of CMC-Se (d). ROS responsive capability of CMC-Se (e).

synthesis of CMC-Se. The structure of CMC-Se was further confirmed by infrared (IR) spectroscopy and X-ray photoelectron spectroscopy (XPS). As shown in Fig. 1a, the IR spectrum of CMC-Se exhibited characteristic peaks at 1690.88 cm^{-1} for the amide bond,[7] 552.95 cm^{-1} for Se–Se bonds, and 1233.9 cm^{-1} and 951.8 cm^{-1} for C–Se bonds,[8] confirming the successful attachment of Se–NH_2 to CMC-Se. The binding energy of Se–Se was 55.9 eV (Fig. 1b), similar to the previously reported value,[9] again confirming the successful attachment of Se–NH_2 to CMC-Se. The morphology of CMC-Se was confirmed by TEM (Fig. 1c), which showed a spherical morphology with selenium primarily distributed around the spheres, accounting for 4.68% of the elemental mass. The mean diameter of CMC-Se was 310.7 nm with a negative zeta potential of −35.67 mV characterized by dynamic light scattering (DLS) as shown in Fig. 1d.

To verify the ROS-responsive properties of CMC-Se, quercetin was loaded into CMC-Se with a loading rate of 4.2% and the *in vitro* quercetin release profile of quercetin@CMC-Se was studied. As shown in Fig. 1e, in oxidative release experiments, the quercetin release rate correlated positively with H_2O_2 concentration, demonstrating the ability of quercetin@CMC-Se to respond to different concentrations of H_2O_2. This allows for precise modulation of drug release according to the severity of inflammation, thereby reducing non-specific drug release and associated risks of side effects. In contrast, quercetin@CMC showed overlapping release curves with the control (Fig. S3, ESI†), confirming that the ROS responsive capability of CMC-Se was introduced by the Se–Se bonds. The ROS-responsiveness of CMC-Se was further verified by FTIR, XPS, and TEM. The characteristic peak of the Se–Se bond of CMC-Se at 552.95 cm^{-1} disappeared, indicating that the Se–Se bond was cleaved by H_2O_2 (Fig. S4a, ESI†). Further detection of selenium binding energy revealed changes in the oxidation state of Se, with spin–orbit coupling analysis indicating a shift in the main peak from 55.9 eV ($3d^5$) to 59.5 eV in the presence of H_2O_2 (Fig. S4b, ESI†). TEM results demonstrated that the originally regular spherical structure of CMC-Se became loose and irregular aggregates after oxidation (Fig. S4c, ESI†). All these results demonstrate that CMC-Se is a highly sensitive ROS nanocarrier that is capable of on-demand drug release in oxidative stressed environments.

Encouraged by the excellent ROS-responsive capability of CMC-Se, we further evaluated its ROS scavenging capability. H_2O_2 was used as representative ROS to stimulate HT-29 cells to simulate oxidative stress cell status. A previous study reported that the concentration of H_2O_2, which can reduce cell viability to approximately 80–90% and significantly increase the ROS level within cells, is considered the ideal concentration for constructing an oxidative stressed cell model.[10] Based on this, treatment with 400 μM H_2O_2 for 4 h can successfully establish an oxidatively stressed cell model in HT-29 cells (Fig. S5, ESI†). The cytotoxicity of CMC-Se was assessed using the Cell Counting Kit-8 (CCK-8) assay. As shown in Fig. S6 (ESI†), concentrations lower than 100 μg mL^{-1} of CMC-Se showed no significant cytotoxicity compared to the control group, which will be selected for further experiments. After finding the safety concentration ranges of CMC-Se and the optimal concentration of H_2O_2 for constructing an oxidatively stressed cell model in HT-29 cells, we further evaluated the ROS scavenging capability of CMC-Se by incubating oxidatively stressed HT-29 cells with different concentrations of CMC-Se, and the intracellular ROS was detected *via* flow cytometry. As shown in Fig. 2a and Fig. S7a (ESI†), the mean fluorescence intensity in the oxidative stress group significantly increased, with a noticeable rightward shift in the fluorescence distribution curve. In contrast, cells treated with CMC-Se showed a gradual decrease in mean fluorescence intensity and a leftward shift in the fluorescence distribution curve; with 50 μg mL^{-1} CMC-Se treatment, intracellular ROS levels were not significantly different from that of the control group. Confocal microscopy images (Fig. 2b) also demonstrated similar results, confirming that CMC-Se effectively removed ROS from cells, and alleviated inflammatory responses. Additionally, flow cytometry analysis and confocal microscopy images with JC-10 staining validated the cytoprotective effects of CMC-Se (Fig. 2c and d). However, CMC could not scavenge intracellular ROS (Fig. S7b and c, ESI†). A similar phenomenon was also shown in Caco-2 cells. Within the safe concentration range of CMC-Se (<600 μg mL^{-1}, Fig. S8a, ESI†) and the optimal concentration of H_2O_2 (800 μM, Fig. S8b and c, ESI†) for constructing an oxidatively stressed cell model in Caco-2 cells, CMC-Se efficiently scavenged intracellular ROS, while CMC exhibited no ROS scavenging capability (Fig. S8d, ESI†). The ROS scavenging capability of CMC-Se may result from a synergistic process involving the reduction of its diselenide bonds, which consumes ROS and glutathione (GSH). This is supported by the ROS and GSH responsive capabilities of CMC-Se (see Fig. 1e and Fig. S9, ESI†) and the observed increases in the enzyme activities of superoxide dismutase (SOD), catalase (CAT), and glutathione peroxidase (GSH-Px) within the oxidatively stressed HT-29 cells (Fig. S10a–c, ESI†). These antioxidant enzymes can act synergistically to effectively eliminate excessive ROS and RNS within cells, preventing cell

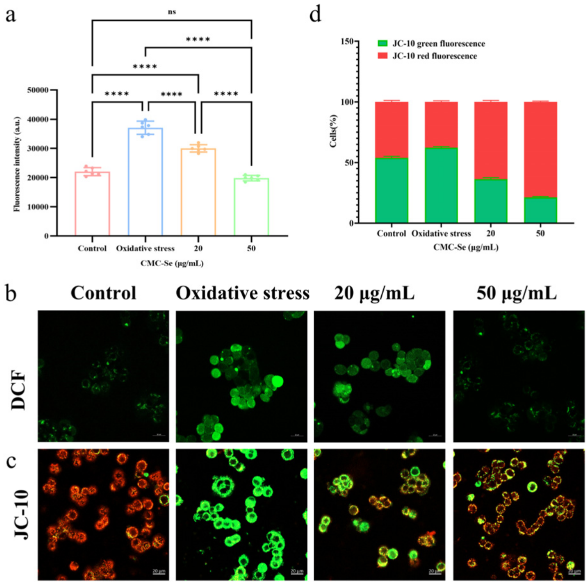

Fig. 2 Flow cytometry analysis of intracellular ROS (a). Confocal microscopy images of ROS and MMP in HT-29 cells. Scale bar: 20 μm (b) and (c). Statistical analysis of cell populations based on b (n = 6) (d).

damage caused by oxidative stress, and thereby safeguarding the health of cells and tissues.[11] Taken together, CMC-Se can effectively clear ROS and alleviate cellular oxidative stress.

To explore why CMC-Se can effectively alleviate cellular oxidative stress, we utilized Cy5.5-labeled CMC-Se and studied its cellular uptake by detecting the fluorescence of Cy5.5 within the cells. As shown in Fig. S11a and b (ESI†), a concentration-dependent cellular accumulation was observed in both normal and oxidatively stressed HT-29 cells. Notably, compared to normal cells, oxidatively stressed cells showed significantly higher uptake of CMC-Se. Furthermore, the saturation uptake concentration was observed to be 50 μg mL^{-1}, after which there was no obvious increase in uptake in either normal or oxidatively stressed cells. Therefore, the cellular uptake concentration of CMC-Se was set as 50 μg mL^{-1}. The CLSM results show similar trends to flow cytometry results (Fig. S12, ESI†), further confirming the above conclusions. The flow cytometry and CLSM results shown in Fig. S13 and S14 (ESI†) clearly demonstrate a time-dependent cellular accumulation, with the highest accumulation observed at 6 h and oxidatively stressed cells again show higher cellular uptake efficiency than normal cells. However, there is no difference in the cellular uptake efficiency of CMC between the normal and oxidatively stressed HT-29 cells (Fig. S15, ESI†). Similar to HT-29 cells, oxidatively stressed Caco-2 cells took up more CMC-Se than normal Caco-2 cells, while there was no difference in the uptake of CMC (Fig. S16, ESI†).

Fluorescence colocalization can be used to study the spatial relationship and potential interactions between two fluorescent molecules in tissues or cells.[12] Therefore, we further utilized fluorescence colocalization to explore the cellular uptake pathway of CMC-Se. As shown in Fig. 3a, the green fluorescence signal of Dio in the cell membrane of oxidatively stressed HT-29 cells colocalized well with the red fluorescence signal of Cy5.5 in CMC-Se, indicating a significant interaction between the cell membrane of oxidatively stressed HT-29 cells and CMC-Se. Further lysosome colocalization analysis revealed that CMC-Se showed significant colocalization with lysosomes after entering the cells (Fig. 3b). A Pearson correlation coefficient (PCC) between 0.5–1.0 indicates colocalization, and additionally, another metric, Manders' correlation coefficient (M1, M2) above 0.5 also indicates colocalization.[12] As shown in Fig. S17a (ESI†), the PCC of CMC-Se with lysosomes was 0.59, and M1 and M2 were both above 0.5. In addition, there was a clear overlap between the fluorescence curves of lysosomes and CMC-Se (Fig. S17b, ESI†), indicating that CMC-Se primarily enters cells *via* vesicle-mediated endocytosis and then is transported to lysosomes. Considering mitochondria are the primary sites of ROS production within cells, we further explore whether CMC-Se can target these sites to exert an antioxidant effect. As shown in Fig. 3c, CMC-Se showed significant colocalization with mitochondria, and the PCC, M1, and M2 values for CMC-Se with mitochondria were 0.66, 0.60, and 0.65, respectively (Fig. S18a, ESI†), indicating that CMC-Se can efficiently accumulate at mitochondria sites. The line profile analysis further supported the results of PCC and MCC analysis (Fig. S18b, ESI†). Taken together, CMC-Se can be efficiently taken up by oxidative-stressed colon cells through close interaction with cell membranes and can accumulate selectively around mitochondrial sites to scavenge excessive ROS, thereby efficiently alleviating cellular oxidative stress.

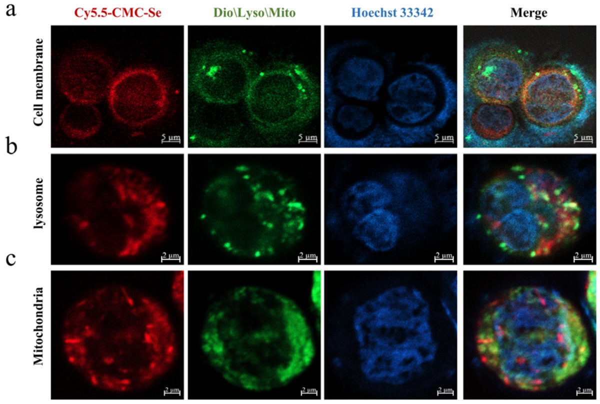

Fig. 3 Co-localization images of the cell membrane (a), lysosome (b), and mitochondria (c). Scale Bar: 2 μm.

To investigate the potential cellular uptake mechanism of CMC-Se, we first evaluated whether CMC-Se was taken up *via* commonly reported endocytic pathways, including macropinocytosis, clathrin-dependent endocytosis, and caveolin-dependent endocytosis. As shown in Fig. S19a and b (ESI†), no significant cellular uptake inhibition was observed even when the concentration of the macropinocytosis inhibitor (ethylisopropylamiloride, EIPA) reached 40 μM, indicating that CMC-Se was not taken up by oxidatively stressed colon cells *via* macropinocytosis. Similarly, pretreatment with a clathrin-mediated endocytosis inhibitor (chlorpromazine) and caveolae-mediated endocytosis (genistein) did not alter the uptake of CMC-Se in oxidatively stressed cells (Fig. S19c–f, ESI†), confirming that clathrin-mediated endocytosis and caveolae-mediated endocytosis are not the primary routes for cellular internalization of CMC-Se. These results suggest that there is a new mechanism mediating

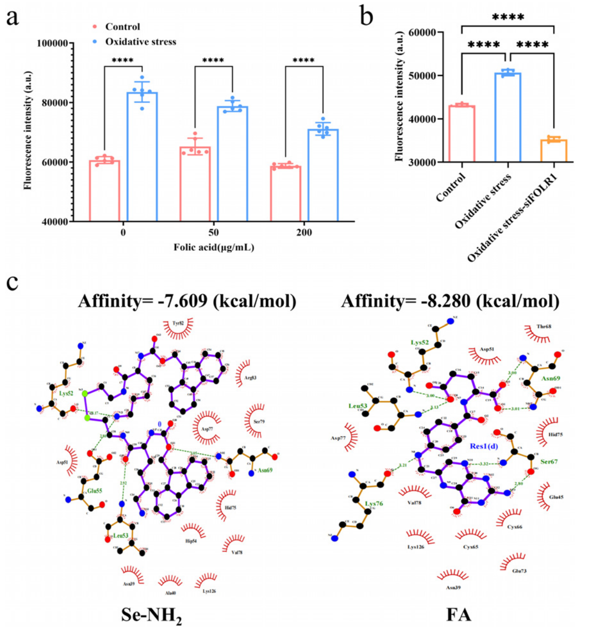

Fig. 4 Average fluorescence quantification of the effect of folate on the cellular uptake (n = 6) (a). Average fluorescence quantification of siFOLR1 effects on the cellular uptake (n = 6) (b). 2D docking model of folate or Se–Se active groups with folate receptor protein (c).

the uptake of CMC-Se by oxidatively stressed colon cells. Therefore, it may be uptaken by other transport proteins. To confirm this guess, we collect the membrane proteins of normal and oxidatively stressed HT-29 cells for proteomic analysis. As shown in Fig. S20a (ESI†), the PCA plot showed a clear clustering between the normal and oxidative stress groups. The oxidative stress group had 1040 differentially expressed proteins (DEPs), with 201 upregulated and 839 downregulated (Fig. S20b, ESI†). DEPs were subjected to GO analysis to select proteins enriched in cell membranes and membrane functions (Fig. S20c, ESI†), and then enriched in the KEGG database for further analysis of specific pathways. Focusing on the transport and metabolic pathways in KEGG (Fig. S20d, ESI†), 61 DEPs were observed. The heatmap revealed the specific conditions of these 61 DEPs (Fig. S20e, ESI†), showing that 9 proteins were significantly upregulated, including FOLR1, PPP2CA, TUBA1C, HSPA2, PEX26, CTSB, ATG13, RAC1, and SOD1. FOLR1 is a high-affinity glycophosphatidylinositol (GPI)-anchored membrane protein that can act as a protein receptor to mediate endocytosis.[13] Therefore, we speculate that the uptake of CMC-Se may be mediated by FOLR1.

To validate this hypothesis, we investigated the effect of folic acid (FA, an inhibitor of FOLR1) on the uptake capacity of HT-29 cells using confocal microscopy and flow cytometry. It was found that the effect of FA on the mean fluorescence intensity of oxidatively stressed cells was significantly higher than that on the mean fluorescence intensity of normal cells (Fig. 4a and Fig. S21, ESI†). With the increasing concentrations of FA, the mean fluorescence intensity of oxidatively stressed HT-29 cells gradually decreased (Fig. S22a and b, ESI†), indicating that the uptake of CMC-Se was mediated by FOLR1. To further verify these results, we employed gene silencing to suppress the expression of FOLR1 in HT-29 cells to investigate the effect of FOLR1 on cellular internalization. As shown in Fig. 4b and Fig. S23 (ESI†), after silencing the FOLR1 gene (Fig. S24, ESI†), the uptake of CMC-Se was significantly inhibited, which further confirms that the uptake of CMC-Se was mediated by FOLR1. Molecular docking analysis revealed that the ROS-responsive component of CMC-Se (Se–Se) and the folic acid show similar binding energy to that of folic acid receptor proteins, and the binding energies are significantly less than -6 kcal mol^{-1}, indicating that there is a close binding potential between CMC-Se and folate receptor proteins (Fig. 4c and Fig. S25, ESI†).

In conclusion, CMC-Se is highly sensitive to ROS and has excellent ROS scavenging activity. In an oxidative stress environment, the FOLR1 protein is highly expressed on the cell membrane of HT-29 cells. CMC-Se, with its specific active sites, can interact with folate receptor proteins through hydrogen bond interactions. This activates the folic acid receptor-mediated endocytic pathway, leading to the high uptake of CMC-Se by oxidatively stressed HT-29 cells.

Conceptualization: Q. Y. and B. B. Z. Methodology: W. L., D. L., J. H., W. D., and Q. Y. Investigation: W. L., D. L., J. H, W. D., and Q. Y. Visualization: W. L., D. L., J. H., W. D., and Q. Y. Validation: W. L., D. L., J. H., W. D., B. B. Z. and Q. Y. Supervision: Q. Y. and B. B. Z. Writing – original draft: W. L. and Q. Y. Writing – review and editing: W. L., B. B. Z., and Q. Y.

This work was financially supported by the National Natural Science Foundation of China (32302280); Special Funding Program for Guangdong Science and Technology Innovation Strategic Project (STKJ202209022); and Research Start-up Foundation of Shantou University (NTF22003).

Data availability

The data supporting this article have been included as part of the ESI.†

Conflicts of interest

There are no conflicts to declare.

Notes and references

1 Y. Gao, R. Yang, Z. Shou, X. Zan and S. Tang, *Chem. Commun.*, 2024, **60**, 6683–6686.
2 W. Y. Li, J. L. Kan, J. J. Wan, Y. A. Li, T. Song, B. Wang, Q. Guan, L. L. Zhou and Y. B. Dong, *Chem. Commun.*, 2023, **59**, 5423–5426.
3 T. Li, S. Pan, S. Gao, W. Xiang, C. Sun, W. Cao and H. Xu, *Angew. Chem., Int. Ed.*, 2020, **59**, 2700–2704.
4 G. Saravanakumar, J. Kim and W. J. Kim, *Adv. Sci.*, 2017, **4**, 1600124.
5 B. Xianyu, S. Pan, S. Gao, H. Xu and T. Li, *Small*, 2024, **20**, 2306225.
6 J. Mosquera, I. García and L. M. Liz-Marzán, *Acc. Chem. Res.*, 2018, **51**, 2305–2313.
7 Y. J. Jo, M. Gulfam, S. H. Jo, Y. S. Gal, C. W. Oh, S. H. Park and K. T. Lim, *Carbohydr. Polym.*, 2022, **286**, 119303.
8 J. Wang, J. Liu, D. Q. Lu, L. Chen, R. Yang, D. Liu and B. Zhang, *Carbohydr. Polym.*, 2022, **292**, 119699.
9 S. Gao, T. Li, Y. Guo, C. Sun, B. Xianyu and H. Xu, *Adv. Mater.*, 2020, **32**, 1907568.
10 J. Xu, T. Chu, T. Yu, N. Li, C. Wang, C. Li, Y. Zhang, H. Meng and G. Nie, *ACS Nano*, 2022, **16**, 13037–13048.
11 K. Jomova, S. Y. Alomar, S. H. Alwasel, E. Nepovimova, K. Kuca and M. Valko, *Arch. Toxicol.*, 2024, **98**, 1323–1367.
12 A. M. Moreno-Echeverri, E. Susnik, D. Vanhecke, P. Taladriz-Blanco, S. Balog, A. Petri-Fink and B. Rothen-Rutishauser, *J. Nanobiotechnol.*, 2022, **20**, 464.
13 M. Scaranti, E. Cojocaru, S. Banerjee and U. Banerji, *Nat. Rev. Clin. Oncol.*, 2020, **17**, 349–359.